Exploring Exciton Relaxation and Multiexciton Generation in PbSe Nanocrystals Using Hyperspectral Near-IR Probing

Itay Gdor,[†] Hanan Sachs,[†] Avishy Roitblat,[†] David B. Strasfeld,[‡] Moungi G. Bawendi,[‡] and Sanford Ruhman[†,*]

[†]Institute of Chemistry and the Farkas Center for Light Induced Processes, The Hebrew University, Jerusalem 91904, Israel and [‡]Department of Chemistry, Massachusetts Institute of Technology, 77 Massachusetts Avenue, Cambridge, Massachusetts 02139, United States

ABSTRACT Hyperspectral femtosecond transient absorption spectroscopy is employed to record exciton relaxation and recombination in colloidal lead selenide (PbSe) nanocrystals in unprecedented detail. Results obtained with different pump wavelengths and fluences are scrutinized with regard to three issues: (1) early subpicosecond spectral features due to "hot" excitons are analyzed in terms of suggested underlying mechanisms; (2) global kinetic analysis facilitates separation of the transient difference spectra into single, double, and triple exciton state contributions, from which individual band assignments can be tested; and (3) the transient spectra are screened for signatures of multiexciton generation (MEG) by comparing experiments with excitation pulses both below and well above the theoretical threshold for multiplication. For the latter, a recently devised ultrafast pump–probe spectroscopic approach is employed. Scaling sample concentrations and pump pulse intensities inversely with the extinction coefficient at each excitation wavelength overcomes ambiguities due to direct multiphoton excitation, uncertainties of absolute absorption cross sections, and low signal levels. As observed in a recent application of this method to InAs core/shell/shell nanodots, no sign of MEG was detected in this sample up to photon energy 3.7 times the band gap. Accordingly, numerous reports of efficient MEG in other samples of PbSe suggest that the efficiency of this process varies from sample to sample and depends on factors yet to be determined.

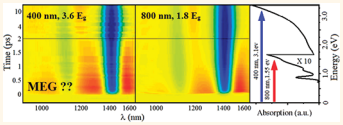

KEYWORDS: quantum dots · multiexciton generation · carrier multiplication · ultrafast spectroscopy · exciton cooling

Transient absorption spectroscopy (TA) has been employed with great benefit in recent years to follow "excitonics" in semiconductor nanocrystals.[1–5] Starting with cooling of the photogenerated carriers, followed by Auger recombination from multiexcitons (MX) to single excitons (SX), and ending with radiative recombination, this sequence of events has been scrutinized extensively by TA to reveal the mechanistic details involved. The former has been discussed in terms of biexciton interactions which shift absorption of already excited nanocrystals to longer wavelengths, along with effects of state filling which blocks transitions involving already occupied states.

The TA method also provides measures for evaluating the related process of carrier multiplication (CM), whereby the absorbance of a single photon leads to the generation of more than one electron–hole pair in a semiconductor. This phenomenon is of great interest to scientists and engineers searching for sources of renewable energy due to its potential for increasing the efficiency of photovoltaic devices. However, the quantum yield of CM in bulk semiconductors is quite low for ambient solar radiation,[6–8] rendering it practically irrelevant for improving the performance of photocells. In recent years, highly efficient CM in various semiconductor quantum dots (QD) has been reported for moderate excess photon energies.[9–13] In one case, the production of seven excitons from a single photon was reported, constituting nearly 100% conversion of the photon energy into excitons. Since quantum confinement forces proximity on the carriers, in QDs, it is more commonly coined multiexciton generation or MEG.

The apparent enhancement of MEG efficiency in nanocrystals has led, in accord with early predictions by Nozik,[14] to the proposal of QD-based photovoltaics as a means of exceeding the Shockley–Queisser limit[15] and more efficient conversion of solar energy into EMF.[16–19] However, the high efficiency of MEG in quantum dots has not been uniformly confirmed. Some studies carried out on the same materials have uncovered much lower yields and, in some cases, no signs of MEG at all, even for

* Address correspondence to sandy@fh.huji.ac.il.

Received for review January 13, 2012 and accepted March 5, 2012.

Published online March 05, 2012
10.1021/nn300184n

excitation well above the reported energy thresholds for its onset.[20,21] Others have directly compared MEG in QDs to that in the bulk, concluding that quantum confinement does not enhance it at all.[22] Thus, despite numerous studies aimed at clarifying this issue, no consensus on the levels of apparent enhancement of MEG in QD samples has emerged.

Quantification of MEG efficiency has been based primarily on the decay kinetics of excitons, detected by ultrafast pump−probe or time-resolved emission spectroscopies. Quantum confinement of carriers in QDs leads to a steep rise in Auger recombination rates with the number of excitons.[23,24] Assuming that exciton annihilation takes place one at a time, the relative amplitudes of the separable stages of exciton decay can be translated into an initial distribution of exciton number states, from which MEG efficiency can be estimated. Inherent difficulties with this approach are (a) that multiple exciton states can also be generated by direct absorption of more than one photon, and (b) that QD cross sections of absorption rise steeply with photon energy, rapidly restricting the pump fluence for which direct multiphoton absorption can be ignored.

In order to account for these difficulties, a novel pump−probe procedure was applied by Ruhman and co-workers to detect the occurrence of MEG in InAS core/shell/shell QDs.[25] Briefly, to compare exciton state distributions generated at two different excitation wavelengths, aiming to quantify MEG, one has to verify that the distribution of absorbed photons is identical at both photon energies. As detailed in ref 25, this can be guaranteed by preparing samples of identical optical density at each pump wavelength (Figure 1) and comparing experiments for which $J\varepsilon_{\lambda_1} = J\varepsilon_{\lambda_2}$, where J is the pump fluence and ε the extinction coefficient at the designated pump wavelength. Notice that this does not require knowledge of absolute cross sections for absorption, only ratios thereof. This approach also eliminates the need for optically thin samples, which produce inherently weak signals.

Using this method, two InAs Core/shell/shell samples were shown to be free of detectable levels of MEG, up to photon energies which exceeded the band-edge nearly 4-fold. Since the publication of those results, numerous additional studies have been published concerning MEG efficiency in QDs, mainly involving lead chalcogenides.[26−28] Most report MEG yields considerably below early estimates, but nearly all observe definite signatures of MEG at photon energies above $h\nu \sim 2.5$ times the band-edge energy. At the same time, this renewed scrutiny has also yielded suggestions that details of surface passivation and chemical treatment can influence MEG yields significantly, and that photoinduced charging of a repeatedly excited sample can give rise to false multiexciton decay patterns which masquerade as MEG.[29−31]

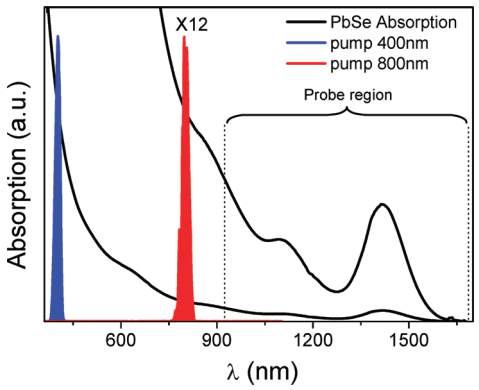

Figure 1. Absorption spectra of the PbSe QDs, along with intensity spectra of the excitation pulses at 800 and 400 nm.

In the present study, TA following femtosecond photoexcitation of freshly prepared colloidal PbSe QDs is followed using multichannel or hyperspectral detection of broad-band NIR probe pulses. As in the case of molecular systems, this approach has proven to be advantageous in applications to NC excitonics since it simultaneously optimizes time and frequency resolution and overcomes the mixing of spectral shifting and population dynamics which is inherent to single-channel detection. Analysis of the collected spectra is conducted with respect to relaxation and recombination of the photogenerated excitons. From it, a detailed characterization of cooling effects on the TA of nascent excitons is obtained. In addition, the extraction of difference spectra associated with various MX states, along with their Auger decay rates, is performed and used to test the identity of individual bands comprising the QD absorption spectrum, as well as to measure the biexciton interactions involved in the probing of each.

Finally, it is also used to test for MEG in this sample as described above. The InAs core/shell/shell samples previously studied are known to be exceptionally well-passivated, as attested to by their high emission quantum yield. This may render those samples poor representatives for characterizing MEG behavior of colloidal QDs, in general, if indeed such generalizations are meaningful. The current study was undertaken in order to determine whether the negative results obtained earlier carry over to other and more extensively studied QD samples. Results obtained using the pump−probe approach described above demonstrate that, in the PbSe sample studied here, no MEG is detected, even with pump photons reaching 3.7 times the band gap energy. Furthermore, by following not only the decay kinetics but also the absolute signal levels, permanent charging effects on the data can be ruled out.

RESULTS

Transient Absorption. As reported in previous studies, the prominent band-edge absorption feature, in our case centered at 1420 nm, involves transition to a state

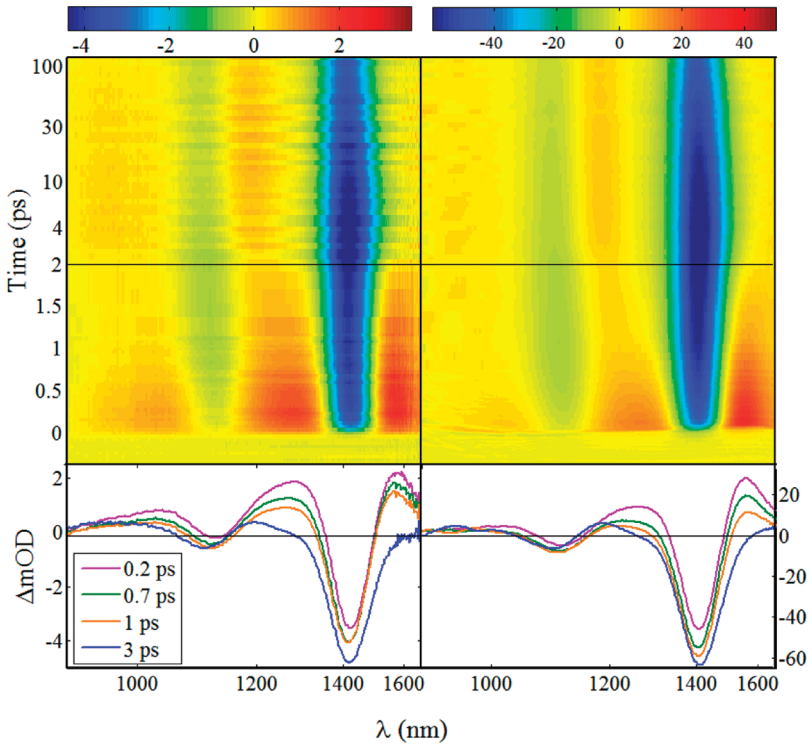

Figure 2. Transient difference spectra presented above as color-coded ΔOD maps and below as temporal cuts at the designated pump−probe delays, after excitation at 400 and 800 nm on the left and right, respectively.

where both electron and hole have a 1S envelope function, designated as $1S_h1S_e$. The assignment of the second absorption peak is not as clear and is debated in the literature, being assigned to transitions to the forbidden $1S_h1P_e/1P_h1S_e$ states[32,33] or alternatively to one reaching the $1P_h1P_e$ state.[34,35] At shorter wavelengths, separation of the optical density into individual transitions becomes more difficult, and only faint spectral features are discernible on a steep exponentially rising absorptive background.

Figure 2 shows the transient difference spectrum recorded after photoexcitation at time $t = 0$ of these PbSe QDs with femtosecond pulses centered at 800 nm (right) and 400 nm (left). Pump photon fluxes in both were controlled to deposit two excitons per QD on average ($\eta = 2$) at the front surface of the sample, and in both samples the OD at the pump wavelength was adjusted to 0.7. Top panels present color-coded ΔOD maps, with the initial 2 ps presented on a linear time scale, and the remainder plotted against $\log_{10}(t)$. A sequence of temporal cuts in the data covering the initial 3 ps of pump−probe delay is also displayed below, covering the cooling of energetic excitons generated by photons containing 1.9 and 3.8 times the particle band gap energy.

Excitation with the pump pulse causes changes in probe transmission throughout the range of initial absorption and extending somewhat to longer wavelengths, as well. They consist mainly of a sharp buildup of enhanced transmission centered near the initial band-edge absorption peak, superimposed on a broad absorption which extends to longer wavelengths, but is apparent throughout. This early difference spectrum resembles a second derivative of the ground state OD, in accordance with earlier TA experiments on various samples of QDs including PbS, where excitation is conducted with photon energies well above the absorption band-edge.[1,36,37] In particular, this includes a buildup of excess absorption below the band-edge, which has recently been the subject of specific study.[38] While the said resemblance was assigned in early studies to an intraparticle stark shifting, more recent studies portray it in terms of biexciton binding effects.[17,39,40]

These features evolve within picoseconds as the nascent excitons cool. The changes observed consist mainly of a disappearance of the broad absorption background, leaving behind the excess transmission feature at the band-edge, as well as a zero integral peak shift signature associated with the second absorption band at ~1100 nm.[35] After this initial rapid stage of evolution, at much longer delay times, a gradual decay of ΔOD across the board is observed, leveling off after a delay of ~100 ps. This is the expected signature of exciton annihilation in crystallites which are initially excited with more than a single photon, due to Auger recombination.[23,24] The prominence of this stage of evolution is dependent upon the pump photon flux, which determines the distribution of exciton number states generated. To demonstrate this, Figure 3 brings spectral cuts in a series of data sets obtained with

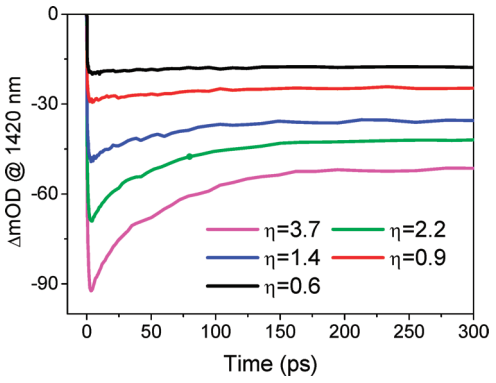

Figure 3. Band-edge transient bleach scans after excitation at 800 nm with the designated front surface fluences in units of photons per absorption cross section. See text for details.

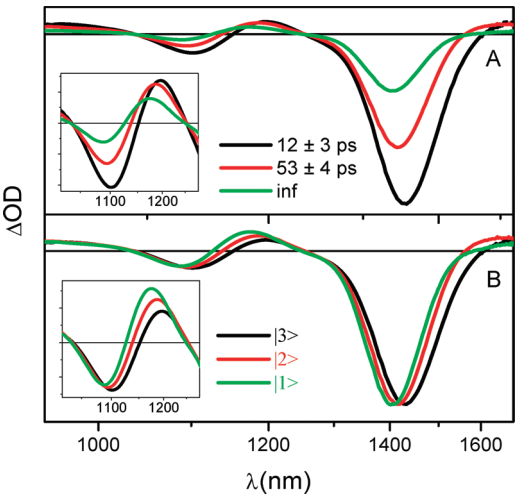

Figure 4. SADS along with associated lifetimes after excitation at 800 nm (A) and after normalizing to the number of excitons (B). Insets: enlargement of the second transition region.

800 nm pump pulses of varying fluence. These are designated in terms of the estimated photon flux–cross section product at the front surface of the sample cell, η. Clearly, at the lowest pump fluence, the induced bleach is essentially constant and free of MX recombination effects. It is important to stress that, since the samples are optically thick, the designated values of η represent only the upper limit this measure takes as the pump traverses the cell. Finally, following Auger recombination, a long-lived difference spectrum characteristic of singly excited QDs remains, which does not decay significantly in our observation window since radiative recombination takes place on hundreds of nanoseconds.

Global Kinetic Analysis. In an effort to separate the contributions to the transient spectra of various multiexciton states, 800 nm pump data were collected at various pump photon densities, and the data at delays beyond the first 3 ps were globally fit to a sequential kinetic scheme including convolution with a Gaussian instrument response function and phases of exponential spectral evolution. The discarded delay range is dominated by exciton cooling not covered in the kinetic scheme. The model expected to account for the dynamics of a mixed initial combination of multiply excited QDs, can be summarized as

$$|N\rangle \rightarrow |N-1\rangle \rightarrow \cdots\cdots |3\rangle \rightarrow |2\rangle \rightarrow |1\rangle \qquad (1)$$

with $|3\rangle$ being the highest initial occupation number considered. The initial distribution of exciton occupation must be known to perform this analysis. For known fluxes, the distribution of the exciton follows the Poisson distribution:

$$\frac{\rho_N}{\sum_N \rho_N} = \frac{e^{-\eta}\eta^{(N-1)}}{N!};\ \eta \equiv \sigma J \qquad (2)$$

where ρ_N is the density per unit area of the N exciton state ($|N\rangle$) and η is the product of σ, the absorption cross section, with J the density per unit area of photons. The influence of sample OD on the flux has to be taken into consideration and thus the distribution can be calculated by the integral:[25]

$$\rho_N = \frac{1}{\sigma}\int_{\eta_0}^{\eta_\infty} \frac{e^{-\eta}\eta^{(N-1)}d\eta}{N!} \qquad (3)$$

This integral disregards MEG in accordance with its application to experiments conducted with 800 nm pump pulses. Our disregard for excited states above $|3\rangle$ stems from the low probability for higher excitation and the rapid growth of Auger recombination rates with N. We have accordingly assumed that all higher excited states have decayed to $|3\rangle$ during the initial 3 ps of delay.

Results of this analysis are presented in Figure 4A in the form of species associated difference spectra (SADS). These are the spectra associated with the three lowest exciton states appearing in scheme 1. The lifetimes associated with each are depicted in the figure. Since the SX state does not decay within our observation window, its lifetime is designated as infinite (Inf). As expected, the band-edge bleach appears to scale with the number of excitons, each accounting for ~0.25 of the initial absorption. This is even clearer in panel B of Figure 4, where the same spectra have been divided by the occupation number before comparison. It also serves to demonstrate the systematic red shifting in this bleach as the occupation number mounts and a concomitant red shift in the first derivative signature surrounding the second absorption peak near 1100 nm, which can be gauged by the changing crossing point on the x axis.

Testing for the Existence of MEG. In a previous investigation,[25] the existence of MEG in InAs core/shell/shell QDs was tested and found to be absent by comparing band-edge bleach signals obtained in "equivalent" experiments conducted with different

pump photon energies. The rationale behind this approach was outlined above. Here, hyperspectral probing allows a refinement of that approach, making possible a comparison of the whole transient spectrum immediately after exciton cooling, and following the completion of Auger recombination, for the various photon energies. This provides a superior test since it excludes the possibility that biexciton induced spectral shifts interfere with this comparison.[10,26]

The left panel of Figure 5 depicts such a comparison alongside a more conventional overlay of the kinetics of the band-edge bleach, throughout the decay of multiexcitons. As in the previous study using this approach, a single scaling factor, related to the ratio of the sample absorption cross sections at both excitation wavelengths, brings the spectral and temporal cuts in the two data sets into perfect overlap. In particular, no excess in bleach is observed at early times after 400 nm excitation, which would be indicative of the presence of MEG.

DISCUSSION

Absence of Detectable MEG. A central objective of this study, looking for the existence of observable MEG up to a photon energy level of 3.7 times the band gap, is answered definitively for this sample by the comparison presented in Figure 5. Quantifying MEG efficiencies, had such been detected, would require further assumptions and data manipulation. The satisfactory match of spectra at all delays through the described scaling demonstrates the effective absence of this process up to the photon energies employed, within an uncertainty determined by the S/N levels of ±4%. Even for the most conservative recent estimates, which have factored in all systematic errors detected in the pioneering studies, this limit is exceeded by more than a factor of 4 for equivalent experiments. In fact, this is the only study published to date which reports the absence of MEG under such irradiation conditions.

We have chosen to repeat our search of MEG using our particular method, evading the necessity of measuring vanishingly small signals in order to do this. However, this difference alone, with respect to previous studies of exciton dynamics in lead chalcogenide QDs, cannot explain the divergence of conclusions. Numerous recent studies have commented on the effects of surface chemical treatment, including exposure to air, on the apparent levels of MEG in nanocrystals.[28−31,36,41,42] In this respect, we emphasize that the sample investigated here had been synthesized weeks before and handled in standard air and moisture-free environments. The only chemical manipulation involved in our study was dilution with deaerated anhydrous solvent and addition of a small amount of oleic acid to protect the surface passivation of the particles upon dilution. Clearly this study demonstrates

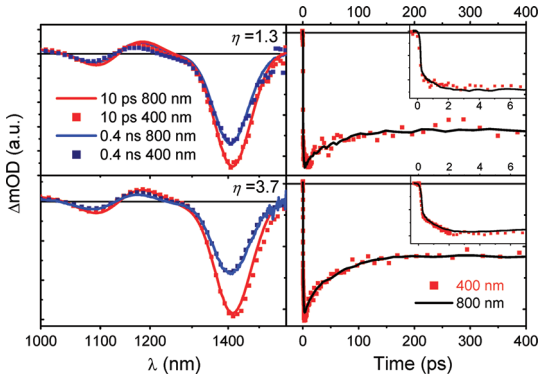

Figure 5. Comparison of equivalent experiments with 800 and 400 nm excitation. Left: transient difference spectra taken at the designated pump−probe delays, with η = 1.3 (above) and η = 3.7 (bellow). Right: comparison of spectral cuts in the data centered at the band-edge absorption feature following 400 nm (red squares) and 800 nm (solid lines) at two pump fluences. Insets detail the initial 6 ps of the data.

that significant additional fundamental research into identifying the factors which underlie the different levels and thresholds of MEG in nanocrystals is required before it can be applied systematically in the conversion of solar energy.[43]

Exciton Cooling Dynamics. Exciton cooling during the first few picoseconds following above band-edge excitation leads to continuous spectral evolution of pump−probe data at the long wavelength end of the QD spectrum. As stated in the introduction, these features have been assigned to a combination of spectral shifts, giving way to transition bleaching due to state filling as the carriers relax to the band-edge.[1,35−37] Short-lived shifts in the well-defined bands near the absorption onset, interpreted alternatively in terms of intraparticle Stark shifts or biexciton binding energies associated with the probe transition, have been reported to produce difference spectra resembling a second derivative of the linear absorption spectrum. Some aspects of the temporal cuts at the bottom of Figure 2 qualitatively match this description, with the prominent excess absorption feature at energies below the band-edge being the most conspicuous. Clearly, at a delay of 3 ps, regardless of the excess energy of pump photons, a transition to net bleaching at the band-edge is also apparent. Other noteworthy observations from the sequence of cuts are (1) that, at both pump wavelengths, the transient spectrum at early delays appears as localized bleach bands set on a broad absorptive background extending throughout the probed range, and peaking near the band-edge bleach feature; (2) that this background is broader when exciting with the more energetic photons; and (3) unlike an earlier report from Harbold *et al.*[33] on QDs of PbSe, the band-edge bleach, once subtracted from the decaying absorptive background, rises rapidly and varies marginally in amplitude throughout the process

of exciton cooling, independent of the exciting photon energy. Accordingly, the bleach of the 1S−1S is to a large degree instantaneous, and later growth appears to stem from erasure of the broad absorption feature within a few picoseconds.

To investigate this further, a series of dynamic difference spectra have been extracted from the lowest pump fluence data obtained with excitation at 800 nm. This observable approximates a time derivative of the transient spectrum and presents changes in the sample spectrum taking place over a short delay period. The results are presented in Figure 6 as an overlay, with the period of evolution to which each pertains depicted in the legend. Similar analysis for other pump fluences produces nearly identical results.

The figure justifies the impression concerning early delays being dominated by decay of a broad absorptive background. Indeed, over the first picosecond, the net change at all wavelengths is a reduction in absorption. Along with this general trend, specific structures centered at the prominent ground state absorption bands are observed, demonstrating that erasure of a continuous background is not all that is taking place. Finally, this reduces to continued bleaching in a distinct range to the red of the band-edge absorption and minor enhancement of absorption at the transition above.

Separating this intricate sequence of spectral changes is hampered by the spectral overlap of the individual absorption bands. Dissecting this stage of spectral evolution, in search of all underlying mechanisms, requires a more monodisperse ensemble of particles. In view of said overlap, we turn to the difference dipole strength Δd over the whole probed spectral range, defined as $\Delta d \equiv \int(\Delta\mathrm{OD}(\nu,t)/\nu)\mathrm{d}\nu$, to assess the source of early spectral features accompanying exciton cooling. A result of this analysis is presented in Figure 7 for three different runs, high and low fluence excitations at 800 nm plus one high-fluence experiment with a 400 nm pump. In all three cases, the difference dipole strength starts out positive, that is, reflects a net increase of absorption, which reverts to net bleach within hundreds of femtoseconds. In both cases, the amplitude of initial positive change is on the same order of magnitude as the ultimate net bleach. Furthermore, the trend of this measure is unchanged with the shift in pumping fluence or alternatively in the initial distribution of exciton occupation numbers, as long as the pump wavelength is conserved. It is, however, strongly influenced by the pump wavelength. Excitation at 400 nm leads to a slower change in the sign of $\Delta d(0)$ than that observed when exciting at 800 nm.

This result is at odds with the assumption that the difference spectrum at early delays results exclusively from spectral shifting, which, to a first approximation, redistributes but does not change dipole strength.

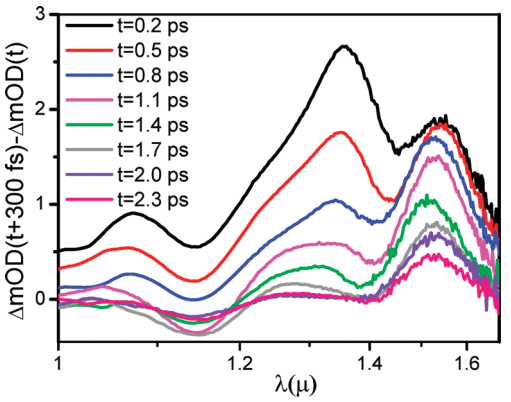

Figure 6. Series of dynamic difference spectra obtained by subtracting the ΔOD data over the interval designated in the legend. This measures the specific spectral change occurring over the designated interval in delay times.

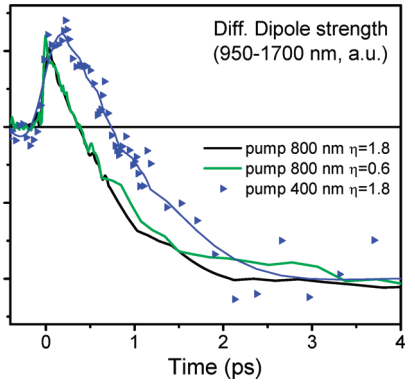

Figure 7. Difference in dipole strength over the recorded spectral range as a function of time evaluated by integration according to $\int(\Delta\mathrm{OD}(\nu,t)/\nu)\mathrm{d}\nu$ *vs* delay (t) for data excited at 800 and 400 nm.

Later on, the effects of state filling are expected to lead to partial bleaching of absorption in the covered region, due to the reduction of the available quantum states. The NIR is also not expected to be influenced by intraband absorption features, which have been shown to be deeper in the mid-IR.[5] So unless these early features reflect intraband transitions, there is a missing part to this puzzle which will require further scrutiny. In any case, it is curious that the transient difference spectra, and accordingly the difference dipole strengths they exhibit, are nearly unchanged upon large variations in pump fluence, in accord with the minute variation of $\Delta\mathrm{OD}(\lambda)/N$ with $|N\rangle$. A similar observation of nearly identical spectral changes accompanying relaxation of hot mono- and multiexcitons has been reported by Jonas *et al.*[42] for above band-edge excitation of PbS QDs. However, that study was limited to following transmission changes high above the band gap throughout, and the relation of such changes to those observed near the absorption onset are yet to be fully understood and are in fact the crux of our dilemmas above.

Global Fitting Results. The kinetic fitting procedure deals with the spectral evolution which supersedes exciton cooling, concentrating on changes brought on by Auger recombination of multiexcitons arising from multiphoton absorption at significant pump fluences. In order to appreciate the significance of the spectra associated with this analysis to mono-, bi-, and triexcitons, it is helpful to reiterate what they represent. They are a subtraction of the linear absorption spectrum of ground state particles and addition of the spectrum of the particular exciton state under study. The trends that arise from this analysis are generally in accord with the report by Trinh *et al.*,[35] who reconstructed similar spectra from multiple single wavelength runs, showing that while the band-edge bleach grows with the number of relaxed excitons, the second peak, which they assign to transitions to the 1P1P hole/electron state, is only shifted to the red due to biexcitonic interactions. This transition accordingly leads to a first derivative contribution. The full spectral coverage, and separation to individual number states, allows finer scrutiny of these trends. First, the band-edge bleach peak red shifts progressively, and its amplitude scales nearly linearly with *N*. The same is true for the red shift of the higher (1P1P) peak. In addition, even after relaxation to the band-edge, all three exciton states extracted show an absorptive contribution to the red of the band-edge.

In order to test whether the amplitudes of these features and their spectral shifts are consistent with the assignment in ref 35, a reconstruction of the SADS in Figure 4 was attempted in the following fashion. The steady state absorption spectrum was shifted by twice the differences in zero crossings near the 1P1P peak in the lower panel of Figure 4 and then spliced with $-N/4$ times the 1S1S band-edge feature. *N* as before represents the number of excitons relevant to each SADS. The results for all three spectra are presented in Figure 8, demonstrating a nearly perfect match with the data. This match underlines the correct previous assignment of this feature and allows a quantitative determination of the biexciton interaction as a linearly additive binding of 130 ± 20 cm^{-1} (16 ± 2 meV). This analysis assumes a constant value for the biexciton attraction following the initial stage of cooling and is considerably larger than found for CdSe NCs of similar size.[44] Unlike the report of Trinh *et al.*,[35] this shift appears to be linear with *N* up to $N = 3$ and is nearly 3 times larger than the value of 6 meV reported there. This may be caused by the enhanced confinement in our smaller particles, but determining that must await a systematic study. Finally, it is interesting to point out that the subtraction described above to simulate the SADS also succeeds in reconstructing the weaker broad features surrounding the derivative-like signature of the 1P1P band, suggesting that, if indeed formally forbidden transitions absorb in this range, their response to the presence of additional excitons may be similar to that of the 1P1P band, as well.

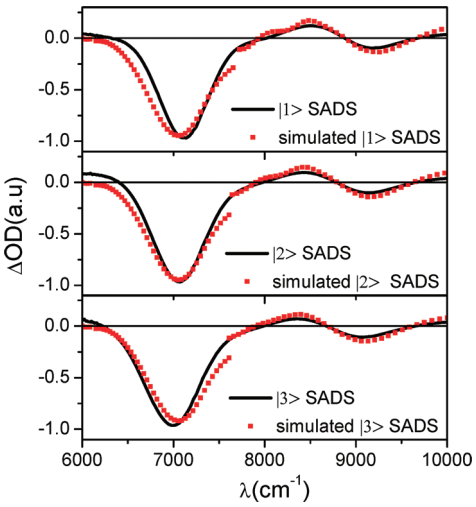

Figure 8. Comparison of the experimental (black line) and simulation (red squares) for all three SADS shown above. Simulation protocol is detailed in the discussion.

CONCLUSIONS

Application of hyperspectral femtosecond transient absorption spectroscopy to the photophysics of PbSe nanocrystals has provided detailed spectral coverage of exciton relaxation and recombination. Initial excitonic cooling following absorption high above the band gap leads largely to erasure of a broad initial pump induced absorption extending throughout the probed region to below the onset of the linear absorption spectrum. Difference dipole strength integration over the full probing range is presented as an alternative measure of the mechanisms giving rise to early spectral features due to hot excitons and shown to raise new riddles in this regard. Kinetic analysis of data obtained with high pump fluences leads to separation of the transient difference spectra into single, double, and triple exciton state contributions. Analysis of their spectral density proves earlier assignments of low-lying 1S1S and 1P1P bands to be correct and quantifies the biexciton shifting energies of the latter to be $N \times 130$ cm^{-1}, where *N* is the number of additional excitons in the QD. Finally, the transient spectra are screened for signatures of multiexciton generation (MEG) by comparing experiments with pump photon energies both below and well above the theoretical threshold for multiplication. This was conducted using a recently devised ultrafast pump–probe spectroscopic approach, where sample concentrations and pump pulse intensities are inversely scaled with the extinction coefficient at each excitation wavelength. This approach was shown to overcome ambiguities due to direct multiphoton excitation, uncertainties of absolute absorption cross sections, and

low signal levels. As observed in that study dedicated to InAs core/shell/shell nanodots, no sign of MEG was detected in the current PbSe sample up to photon energy 3.7 times its band gap. Accordingly, numerous reports of efficient MEG in other samples of PbSe suggest that the efficiency of this process varies from sample to sample and depends on factors yet to be determined.

EXPERIMENTAL METHODS

PbSe nanocrystals, whose absorption spectrum is presented in Figure 1, were prepared as previously described,[21,45] handled in oxygen-free environments, and irradiated in air-tight 1 mm path length optical glass cuvettes. All samples were held at room temperature, and the QD concentrations were adjusted to produce an OD of 0.7 at the excitation wavelengths. The laser system and methods of measurement have been described in detail elsewhere.[46] A few microjoules of the 30 fs amplified output from a homemade multipass titanium sapphire system served to generate a white light continuum probe by focusing in 3 mm of sapphire.

The continuum pulses were collimated and refocused into the sample using reflective optics. Another portion of the amplified fundamental was used to generate pump pulses, either directly at ~1.5 eV or after doubling in 0.1 mm of BBO, and intensity spectra of both are shown in Figure 1, as well. Scans on a thin silicon wafer provided the probes' wavelength-dependent group delay. After the sample, the probe pulses were collected with reflective optics into an InGaAs PD array spectrometer (BTC261E, BWTek) alternately with and without sample pumping. Subtraction of these produced the time-dependent difference spectra displayed below, which have been corrected for the measured probe group delay by data interpolation and wavelength-dependent shifting of the time axis.

Conflict of Interest: The authors declare no competing financial interest.

Acknowledgment. This work was supported by the James Franck program for laser matter interactions, and the Israel Science Foundation. The ISF is administered by the Israel Academy of Sciences and the Humanities. The Farkas Center is supported by the Minerva Gesellschaft, GmbH, Munich, Germany.

REFERENCES AND NOTES

1. Klimov, V. I. Optical Nonlinearities and Ultrafast Carrier Dynamics in Semiconductor Nanocrystals. *J. Phys. Chem. B* **2000**, *104*, 6112–6123.
2. Klimov, V. I. Spectral and Dynamical Properties of Multiexcitons in Semiconductor Nanocrystals. *Annu. Rev. Phys. Chem.* **2007**, *58*, 635–673.
3. Nozik, A. J.; Beard, M. C.; Luther, J. M.; Law, M.; Ellingson, R. J.; Johnson, J. C. Semiconductor Quantum Dots and Quantum Dot Arrays and Applications of Multiple Exciton Generation to Third-Generation Photovoltaic Solar Cells. *Chem. Rev.* **2010**, *110*, 6873–6890.
4. Kambhampati, P. Unraveling the Structure and Dynamics of Excitons in Semiconductor Quantum Dots. *Acc. Chem. Res.* **2011**, *44*, 1–13.
5. Wehrenberg, B. L.; Wang, C.; Guyot-Sionnest, P. Interband and Intraband Optical Studies of PbSe Colloidal Quantum Dots. *J. Phys. Chem. B* **2002**, *106*, 10634–10640.
6. Wolf, M.; Brendel, R.; Werner, J. H.; Queisser, H. J. Solar Cell Efficiency and Carrier Multiplication in $Si_{1-x}Ge_x$ Alloys *J. Appl. Phys.* **1998**, *83*, 4213–4221.
7. Robbin, D. J. Aspects of the Theory of Impact Ionization in Semiconductors. *Phys. Status Solidi* **1980**, *97*, 9–50.
8. Smith, A.; Dutton, D. Behavior of Lead Sulfide Photocells in the Ultraviolet. *J. Opt. Soc. Am.* **1958**, *48*, 1007–1009.
9. Schaller, R. D.; Klimov, V. I. High Efficiency Carrier Multiplication in PbSe Nanocrystals: Implications for Solar Energy Conversion. *Phys. Rev. Lett.* **2004**, *92*, 186601.
10. Ellingson, R. J.; Beard, M. C.; Johnson, J. C.; Yu, P.; Micic, O. I.; Nozik, A. J.; Shabaev, A.; Efros, A. L. Highly Efficient Multiple Exciton Generation in Colloidal PbSe and PbS Quantum Dots. *Nano Lett.* **2005**, *5*, 865–871.
11. Schaller, R. D.; Sykora, M.; Pietryga, J. M.; Klimov, V. I. Seven Excitons at a Cost of One: Redefining the Limits for Conversion Efficiency of Photons into Charge Carriers. *Nano Lett.* **2006**, *6*, 424–429.
12. Schaller, R. D.; Petruska, M. A.; Klimov, V. I. Effect of Electronic Structure on Carrier Multiplication Efficiency: Comparative Study of PbSe and CdSe Nanocrystals. *Appl. Phys. Lett.* **2005**, *87*, 253102.
13. Schaller, R. D.; Pietryga, J. M.; Klimov, V. I. Carrier Multiplication in InAs Nanocrystal Quantum Dots with an Onset Defined by the Energy Conservation Limit. *Nano Lett.* **2007**, *7*, 3469–3476.
14. Nozik, A. J. Quantum Dot Solar Cells. *Physica E* **2002**, *14*, 115–120.
15. Shockley, W.; Queisser, H. J. Detailed Balance Limit of Efficiency of p–n Junction Solar Cells. *J. Appl. Phys.* **1961**, *32*, 510–519.
16. Beard, M. C.; Ellingson, R. J. Multiple Exciton Generation in Semiconductor Nanocrystals: Toward Efficient Solar Energy Conversion. *Laser Photonics Rev.* **2008**, *2*, 377–399.
17. Klimov, V. I. Spectral and Dynamical Properties of Multiexcitons in Semiconductor Nanocrystals. *Annu. Rev. Phys. Chem.* **2007**, *58*, 635–673.
18. Semonin, O. E.; Luther, J. M.; Choi, S.; Chen, H. Y.; Gao, J.; Nozik, A. J.; Beard, M. C. Peak External Photocurrent Quantum Efficiency Exceeding 100% *via* MEG in a Quantum Dot Solar Cell. *Science* **2011**, *334*, 1530–1533.
19. Aerts, M.; Suchand Sandeep, C. S.; Gao, Y.; Savenije, T. J.; Schins, J. M.; Houtepen, A. J.; Kinge, S.; Siebbeles, L. D. A. Free Charges Produced by Carrier Multiplication in Strongly Coupled PbSe Quantum Dot Films. *Nano Lett.* **2011**, *11*, 4485–4489.
20. Nair, G.; Bawendi, M. G. Carrier Multiplication Yields of CdSe and CdTe Nanocrystals by Transient Photoluminescence Spectroscopy. *Phys. Rev. B* **2007**, *76*, 081304.
21. Nair, G.; Geyer, S. M.; Chang, L.; Bawendi, M. G. Carrier Multiplication Yields in PbS and PbSe Nanocrystals Measured by Transient Photoluminescence. *Phys. Rev. B* **2008**, *78*, 125325.
22. Pijpers, J. J. H.; Ulbricht, R.; Tielrooij, K. J.; Osherov, A.; Golan, Y.; Delerue, C.; Allan, G.; Bonn, M. Assessment of Carrier-Multiplication Efficiency in Bulk PbSe and PbS. *Nat. Phys.* **2009**, *5*, 811–814.
23. Klimov, V. I.; Mikhailovsky, A. A.; McBranch, D. W.; Leatherdale, C. A.; Bawendi, M. G. Quantization of Multiparticle Auger Rates in Semiconductor Quantum Dots. *Science* **2000**, *287*, 1011–1013.
24. Klimov, V. I.; McGuire, J. A.; Schaller, R. D.; Rupasov, V. I. Scaling of Multiexciton Lifetimes in Semiconductor Nanocrystals. *Phys. Rev. B* **2008**, *77*, 195324.
25. Ben-Lulu, M.; Mocatta, D.; Bonn, M.; Banin, U.; Ruhman, S. On the Absence of Detectable Carrier Multiplication in a Transient Absorption Study of InAs/CdSe/ZnSe Core/Shell1/Shell2 Quantum Dots. *Nano Lett.* **2008**, *8*, 1207–1211.
26. Trinh, M. T.; Houtepen, A. J.; Schins, J. M.; Hanrath, T; Piris, J.; Knulst, W.; Goossens, A.; Siebbeles, L. D. A. In Spite of Recent Doubts Carrier Multiplication Does Occur in PbSe Nanocrystals. *Nano Lett.* **2008**, *8*, 1713–1718.
27. Ji, M.; Park, S.; Connors, S. T.; Mokari, T.; Cui, Y.; Gaffney, K. J. Efficient Multiple Exciton Generation Observed in Colloidal PbSe Quantum Dots with Temporally and Spectrally

Resolved Intraband Excitationv. *Nano Lett.* **2009**, *9*, 1217–1222.
28. Hardman, S. J. O.; Graham, D. M.; Stubbs, S. K.; Spencer, B. F.; Seddon, E. A.; Fung, H.; Gardonio, S.; Sirotti, F.; Silly, M. G.; Akhtar, J.; *et al.* Electronic and Surface Properties of PbS Nanoparticles Exhibiting Efficient Multiple Exciton Generation. *Phys. Chem. Chem. Phys.* **2011**, *13*, 20275–20283.
29. McGuire, J. A.; Sykora, M.; Joo, J.; Pietryga, J. M.; Klimov, V. I. Apparent *versus* True Carrier Multiplication Yields in Semiconductor Nanocrystals. *Nano Lett.* **2010**, *10*, 2049–2057.
30. Midgett, A. G.; Hillhouse, H. W.; Huges, B. K.; Nozik, A. J.; Beard, M. C. Flowing *versus* Static Conditions for Measuring Multiple Exciton Generation in PbSe Quantum Dots. *J. Phys. Chem. C* **2010**, *114*, 17486–17500.
31. Tyagi, P.; Kambhampati, P. False Multiple Exciton Recombination and Multiple Exciton Generation Signals in Semiconductor Quantum Dots Arise from Surface Charge Trapping. *J. Chem. Phys.* **2011**, *134*, 094706.
32. Peterson, J. J.; Huang, L.; Delerue, C.; Allan, G.; Krauss, T. D. Uncovering Forbidden Optical Transitions in PbSe Nanocrystals. *Nano Lett.* **2007**, *7*, 3827–3831.
33. Harbold, J. M.; Du, H.; Krauss, T. D.; Cho, K. S.; Murray, C. B.; Wise, F. W. Time-Resolved Intraband Relaxation of Strongly Confined Electrons and Holes in Colloidal PbSe Nanocrystals. *Phys. Rev. B* **2005**, *72*, 195312.
34. Liljeroth, P.; van Emmichoven, P. A. Z.; Hickey, S. G.; Weller, H.; Grandidier, B.; Allan, G.; Vanmaekelbergh, D. Density of States Measured by Scanning-Tunneling Spectroscopy Sheds New Light on the Optical Transitions in PbSe Nanocrystals. *Phys. Rev. Lett.* **2005**, *95*, 086801.
35. Trinh, M. T.; Houtepen, A. J.; Schins, J. M.; Piris, J.; Siebbeles, L. D. A. Nature of the Second Optical Transition in PbSe Nanocrystals. *Nano Lett.* **2008**, *8*, 2112–2117.
36. Nootz, G.; Padilha, L. A.; Levina, L; Sukhovatkin, V.; Webster, S.; Brzozowski, L.; Sargent, E. H.; Hagan, D. J.; Van Stryland, E. W. Size Dependence of Carrier Dynamics and Carrier Multiplication in PbS Quantum Dots. *Phys. Rev. B* **2011**, *83*, 155302.
37. Gesuele, F; Sfeir, M; Koh, W; Murray, C. B.; Heinz, T. F.; Wei Wong C. Ultrafast Supercontinuum Spectroscopy of Carrier Multiplication and Biexcitonic Effects in Excited States of PbS Quantum Dots. *Nano Lett.*, **2011**, DOI: 10.1021/nl2021224.
38. Sewall, S. L.; Franceschetti, A.; Cooney, R. R.; Zunger, A.; Kambhampati, P. Direct Observation of the Structure of Band-Edge Biexcitons in Colloidal Semiconductor CdSe Quantum Dots. *Phys. Rev. B* **2009**, *80*, 081310.
39. Sewall, S. L.; Cooney, R. R.; Anderson, K. E. H.; Dias, E. A.; Sagar, D. M.; Kambhampati, P. State-Resolved Studies of Biexcitons and Surface Trapping Dynamics in Semiconductor Quantum Dots. *J. Chem. Phys.* **2008**, *129*, 084701.
40. Kambhampati, P. Hot Exciton Relaxation Dynamics in Semiconductor Quantum Dots: Radiationless Transitions on the Nanoscale. *J. Phys. Chem. C* **2011**, *115*, 22089–22109.
41. Beard, M. C.; Midgett, A. G.; Law, M.; Semonin, O. E.; Ellingson, R. J.; Nozik, A. J. Variations in the Quantum Efficiency of Multiple Exciton Generation for a Series of Chemically Treated PbSe Nanocrystal Films. *Nano Lett.* **2009**, *9*, 836–845.
42. Cho, B.; Peters, W. K.; Hill, R. J.; Courtney, T. L.; Jonas, D. M. Hot Carrier Dynamics in Lead Sulfide Quantum Dots. *Nano Lett.* **2010**, *10*, 2498–2505.
43. Nair, G.; Chang, L. Y.; Geyer, S. M.; Bawendi, M. G. Perspective on the Prospects of a Carrier Multiplication Nanocrystal Solar Cell. *Nano Lett.* **2011**, *11*, 2145–2151.
44. Sewall, S. L.; Cooney, R. R.; Dias, E. A.; Tyagi, P.; Kambhampati, P. State-Resolved Observation in Real Time of the Structural Dynamics of Multiexcitons in Semiconductor Nanocrystals. *Phys. Rev. B* **2011**, *84*, 235304.
45. Steckel, J. S.; Coe-Sullivan, S.; Bulovic, V.; Bawendi, M. G. 1.3 to 1.55 μm Tunable Electroluminescence from PbSe Quantum Dots Embedded within an Organic Device. *Adv. Mater.* **2003**, *15*, 1862–1866.
46. Wand, A.; Rozin, R.; Eliash, T.; Jung, K. H.; Sheves, M.; Ruhman, S. Asymmetric Toggling of a Natural Photoswitch: Ultrafast Spectroscopy of Anabaena Sensory Rhodopsin. *J. Am. Chem. Soc.* **2011**, *133*, 20922–20932.